Design, Numerical and Experimental Investigation of High Swirling Flow in an Annular Combustion Chamber

Zahra Ghahramani[1], Masoud Zareh[2, *]
Department of Mechanical Engineering,
Science and Research Branch, Islamic Azad University, Tehran, Iran
E-mail: zahra.ghahramani@srbiau.ac.ir, m.zareh@srbiau.ac.ir
*Corresponding author: m.zareh@srbiau.ac.ir

Hossein Pourfarzaneh[3]
Designer head, Farzanegan Propulsion Systems Design Bureau, Iran Rasht
E-mail: Hossein@farzaneganpb.com

Farshad Pazooki[4]
Department of Aerospace Engineering,
Science and Research Branch, Islamic Azad University, Tehran, Iran
E-mail: Pazooki_fa@srbiau.ac.ir

Abstract: In this study, an annular combustion chamber of a turbojet engine with a net trust of 1650N is designed. Kerosene is considered as fuel in this study. The design consists of evaluation of the reference quantities, calculation of the required dimensions, estimation of air distribution and pressure drop, estimation of the number and diameter of air admission holes, as well as aerodynamic considerations. The design process is accompanied by Computational Fluid Dynamics (CFD) based on RANS simulation. Three-dimensional simulation of the reacting process within the combustion chamber is carried out based on the finite volume method. The RNG turbulent model and the finite rate/eddy dissipation combustion model are considered in the present study. Finally, the (atmospheric test) AT rig of the combustion chamber is explained. The Turbine Inlet Temperature (TIT) of combustion chamber is measured at different operating conditions. The TIT values in the numerical simulation and experimental measurement are 1191.1K and 1227 K, respectively, in the design point. The SN and the angle of the RZ are equal to 0.9955 and 35.26 degree, respectively. The temperature, velocity and pressure fields of RZ, air-fuel mixture, combustion turbulence are then presented in image outputs and graphs. The results indicate that the temperature distribution at the outlet of combustion chamber is relatively uniform.

Keywords: Annular Combustion Chamber, Atmospheric Test (AT), 3D Numerical Simulation, Swirler Number (SN),

Biographical notes: Zahra Ghahramani is a PhD student at the Department of Mechanical Engineering, Science and Research Branch, Islamic Azad University, Her current research focuses on combustion in aeroengine. **Masoud Zareh** received his PhD in Mechanical Engineering from Science and Research Branch, Islamic Azad University. He is currently Assistant Professor at the Department of Mechanical Engineering, Science and Research Branch, Islamic Azad University. His current research interest includes CFD and heat transfer. **Hossein Pourfarzaneh** is designer head at Farzanegan Propulsion Systems Design Bureau, Iran. He received his PhD in Mechanical Engineering from Sharif University. **Farshad Pazooki**, received his PhD in Aerospace Engineering from Science and Research Branch, Islamic Azad University. He is currently Assistant Professor at the Department of Aerospace Engineering, Science and Research Branch, Islamic Azad University.

1   INTRODUCTION

The design of the annular combustion chamber is based on different experimental and semi-experimental relationships [1-3]. Design methodologies of combustion chamber have been developed for aeroengine [4-5]. Different methods have been employed for the combustion chamber design, each of which may focus on one or more specific objectives [6-8].

Amani et al [9] studied the optimization multi-objective design in the combustion chamber of a gas turbine based on air partitioning in different zones method. The authors used the Computational Fluid Dynamics (CFD) method and investigated the effect of air partitioning on various parameters such as; maximum outlet temperature and its uniformity and the combustion chamber efficiency. In the final optimal design, these parameters improved by 7%, 5%, and 6%, respectively. Amani et al. [9] concluded that the improved results were due to the flame length decreasing. It is a function of the multiple central Recirculation Zone (RZ) formation. Therefore, the RZ quality is directly related to the swirling flow strength. Powerful swirling flow is one of the basic requirements of diffusion flames in a gas turbine combustion chamber for flame stability [10]. The swirling flow creates a low-pressure central zone which is named Central Recirculation Zone (CRZ). The CRZ improves the fuel and air mixing [11-12]. The vortex breakdown phenomenon is a type of powerful swirling flow that it generates RZ [12]. It creates two rotational flow zones which have negative axial velocity. One zone is produced at the center of the combustion chamber and adjacent to the main axis (IRZ) and the other is located at the upper and lower corners of the combustion chamber (ORZ) [13]. The swirling flow strength is measured by the Swirler Number (SN). It is a dimensionless parameter that measures the rotational flow strength relative to the axial flow strength [14]. It is expressed as follows in Equation (1) [1]:

$$SN = \frac{2G_m}{D_{SW}G_t} \tag{1}$$

G_m, G_t and D_{SW} are axial flux of angular momentum, axial thrust and swirler diameter, respectively in Equation (1). The SN value varies between zero and one. If it is greater than 0.6, the producing swirling flow will be appropriate. Increasing the SN and trying to improve its performance has been considered in various researches [15-16].

There are few works in the literature related to the design methodology focused on reacting flows with the maximum value of SN. Therefore, in this study, design of an annular combustion chamber with high SN configuration is investigated. Therefore, in this study,

design, numerical simulation and experimental investigation of an annular combustion chamber with kerosene as fuel and 1650N thrust in design point are concluded. First, the design methodology is expressed and the problem is raised. Second, the different dimensions are calculated especially Geometry of the Swirler (SW). Then, RANS turbulence model is considered for air- fuel ratio, turbulent combustion and RZ investigation. Finally, the Atmospheric Test (AT) rig of the annular combustion chamber is explained and different operating conditions are investigated.

2   DESIGN METHODOLOGY

The design methodology has been done based on the initial design parameters. These are mostly the compressor exit and turbine inlet constraints. "Table 1" shows the initial parameters used for the design methodology.

Table 1 Initial design parameters

Parameter	Quantity
MFP (mass flow parameter),	0.017
ΔPcc (total pressure loss)	6.5%
(fuel-air ratio) FAR	0.02
(turbine inlet temperature), K TIT	1190
(turbine inlet velocity), ms⁻¹ V_TIV	180

$\dot{m}_{air}$, $T_{tot,in}$ and $P_{tot,in}$ are the inlet air mass flow rate in kg/s, the inlet total temperature in K and the inlet total pressure in KPa. The expression of $\frac{\dot{m}_{air}T_{tot,in}^{0.5}}{P_{tot,in}}$ is named Mass Parameter (MP). It can show the effect of inlet parameters of combustion chamber in one nondimensional parameter [17]. Figure 1 shows the design methodology of the annular combustion chamber, especially in the SW section.

The combustion chamber type is selected based on the inlet parameters such as temperature, pressure and air mass flow rate. Reference area (A_{ref}) and liner area (A_L) are then calculated. Air partitioning in the different zones is done. The SW is designed and its SN is calculated.

Reference area: The Aref has a direct effect on the aerodynamics flow in the combustion chamber [1].
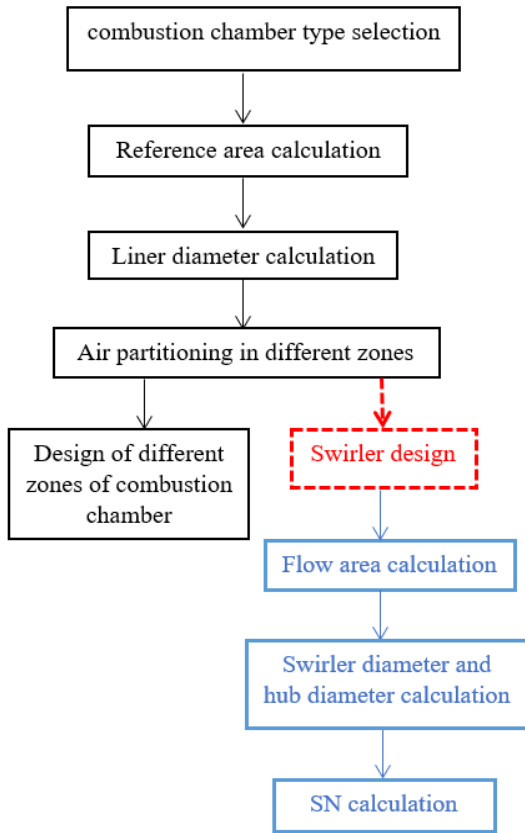
Figure 2 shows the Aref in an annular combustion chamber.
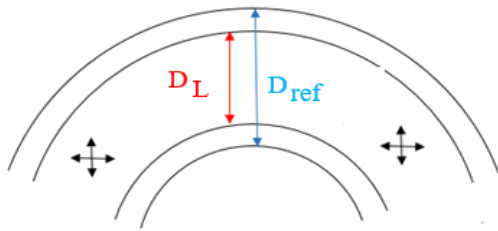
Fig. 1   Design methodology.

Fig. 2   The reference area in an annular combustion chamber.

The Aref is calculated based on Equation (2) [1]:

$$A_{ref} = \left[\frac{R}{2} \left(\frac{\dot{m}_{air} T_{tot,in}}{P_{tot,in}} \right)^{0.5} \frac{\Delta P_{CC}}{q_{ref}} \left(\frac{\Delta P_{CC}}{P_{tot,in}} \right)^{-1} \right]^{0.5} \quad (2)$$

The pressure loss factor $\left(\frac{\Delta P_{CC}}{q_{ref}} \right)$ is equal to 20 in annular combustion chamber [18]. R states the universal gas constant.

A_L is calculated based on Equation (3) [18]. Then liner diameter (D_L) is determined:

$$A_L = 0.7 A_{ref} \quad (3)$$

Air partitioning: The key point for air partitioning in different zone is equivalence ration (φ) of CZ. The φ is defined based on Equation (4) [2]:

$$\varphi = \frac{FAR_{real}}{FAR_{stoich}} \quad (4)$$

The FAR expression refers to fuel air ratio. The applied fuel to the combustion chamber is kerosene, which is estimated with 12 carbon atoms and 23 hydrogen atoms [2]. The stoichiometric reactive mechanism follows Equation (5) [2]:

$$C_{12}H_{23} + \frac{47}{2}(O_2 + 3.76N_2) \Rightarrow$$
$$12CO_2 + \frac{23}{2}H_2O + \frac{23}{2}N_2 \quad (5)$$
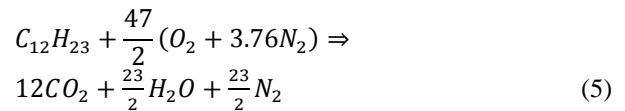
Based on Equation (5), the FARstoich is equal to 0.0688. The maximum value of φ is 1.5 in CZ, so the air partitioning of swirler and PZ is done based on this point [19]. "Table 2" shows air partitioning in different zones of combustion chamber in this research.

Table 2 The air partitioning in different zones

Zone	%air mass flow rate
CZ	20
SZ	12
DZ	68

Different zones: Pattern Factor (PF) is defined as the maximum deviation of the temperature profile of the engine in the worst operating conditions. PF varies between 0.25 to 0.4 in aeroengine and should be estimated in design process of combustion chamber [4]. PF is equal to 0.25 in this research. Liner length (L_L) is calculated based on Equation (6):

$$L_L = \frac{-D_L}{0.05 \frac{\Delta P_b}{q_{ref}} Ln(1-PF)} \quad (6)$$

The L_{PZ}, L_{SZ} and L_{DZ} are calculated based on Equation (7) to (9), respectively [5]:

$$L_{PZ} = \frac{3}{4} D_L \quad (7)$$
$$L_{SZ} = \frac{1}{2} D_L \quad (8)$$
$$L_{DZ} = D_L(3.83 - 11.83PF + 13.4PF^2) \quad (9)$$

Holes: The holes total area follows as Equation (10) [18]. CD is the hole discharge coefficient. It is estimated based on holes type (plain or plunged) [1], [18]. In this research, holes type is plunged and based on reference [1], CD is equal to 0.76:

$$\frac{\Delta P_{hole}}{P_{tot,in}} = \frac{143.5 \dot{m}_{hole}^2 T_{tot,in}}{P_{tot,in}^2 CD^2 A_{hole,tot}^2} \qquad (10)$$

3 SWIRLER DESIGN

The swirlers are divided into two types of axial and radial. In the axial swirler, the blades have a constant angle. Axial swirler has the simpler manufacturing process than radial swirler and it produces less noise which has a direct effect on the combustion stability [1]. In this study, the axial swirler is selected. "Table 3" shows the range of swirler parameters [1]. Geometrical parameters of an axial swirler are shown in "Fig. 3".

Table 3 The required design range parameters of the axial swirler [19]

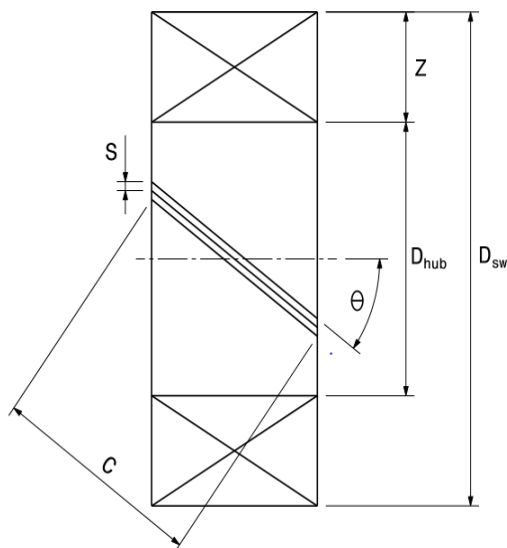| Zone	Range
Angle of vane	30-60 degree
Thickness of vane	0.7-1.5 mm
Vane number	8-16
Swirler pressure loss	3-4% ΔP_{cc}
Shape factor	1.3

Fig. 3 Geometrical parameters of an axial swirler.

Where, D_{sw}, D_{hub} and θ are the swirler diameter, swirler hub diameter and the vane angle, respectively. C and S are the vane characteristics which are named chord and vane space, respectively. Z is the annular space length and it is formed by the swirler hub diameter and the swirler diameter [1]. The required design range parameters of the axial swirler is presented in "Table.3". The most important parameter in SW design is the pressure loss estimation [1], [19]. The pressure loss is estimated at 3% of the inlet total pressure to the combustion chamber in this study. The flow area of the swirler is calculated based on Equation (11) [19]:

$$A_{SW} = A_{ref}^2 K_{SW}^{-1} \left(\frac{\Delta P_{SW}}{q_{ref}} K_{SW}^{-1} \left(\frac{\dot{m}_{air}}{\dot{m}_{SW}} \right)^2 + \left(\frac{A_{ref}}{A_L} \right)^2 \right)^{-1} (\cos\theta)^{-1} \qquad (11)$$

Depending on the swirler flow area, the value of the swirler diameter and the swirler hub diameter are calculated [19]. The D_{SW}/D_h varies between 1.5-3. It is especially estimated based on existence space for swirler geometry. It is equal to 2 in this research. The D_{SW} and D_h are calculated by Equation (12) [19]. n and δ are the number and the thickness of swirler vane:

$$A_{SW} = \frac{\pi}{4}(D_{SW}^2 - D_h^2) - 0.5n\delta(D_{SW} - D_h) \qquad (12)$$

The SN is calculated using Equation (13) [1] and it is equal to 0.9955:

$$SN = \frac{2}{3} \frac{1 - \left(\frac{D_{hub}}{D_{sw}} \right)^3}{1 - \left(\frac{D_{hub}}{D_{sw}} \right)^2} \tan\theta \qquad (13)$$

The magic circles define the RZ. Magic circles are located inside the liner. These circles can capture the RZ flow in the liner length and angle of RZ that are other important factors for checking the CZ which are calculated based on Equation (14) and Equation (15) [20].

$$L_{RZ} = 2 D_{SW} \qquad (14)$$

$$\theta_{RZ} = \cos^{-1}\left(\left(\frac{-D_L(D_L - 2D_{SW})}{2D_L^2 - 4D_L D_{SW} + 4D_{SW}^2 - 8D_L L_{RZ} + 16L_{RZ}^2} \right) - \left(\frac{(D_L^2 - 4D_L D_{SW} + 4D_{SW}^2 - 8D_L L_{RZ} + 16L_{RZ}^2)}{2D_L^2 - 4D_L D_{SW} + 4D_{SW}^2 - 8D_L L_{RZ} + 16L_{RZ}^2} \right) \right) \qquad (15)$$

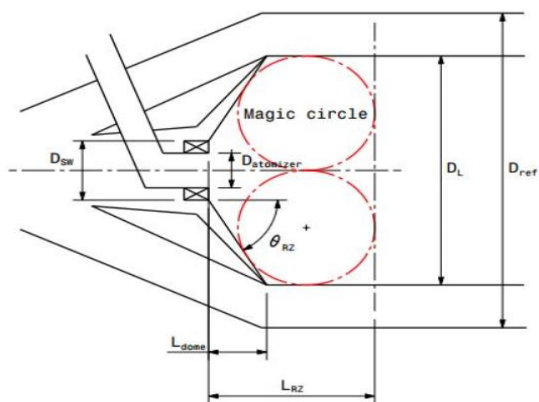The schematic of the RZ is indicated in "Fig 4":

Fig. 4   The magic circles in an annular combustion chamber.

The angle of the RZ is 35.26 degree based on the Equation (15). It is important to estimate the compatibility of atomizer and swirler in the co-flow combustion chamber because of the atomizer limitations.

4   GEOMETRICAL MODEL

Figure 5 shows the annular combustion chamber of a turbojet engine in this research. It is designed based on the methodology which is completely explained in previous parts. It has 12 hollow cone atomizers. There is one row hole in PZ, SZ and DZ. It is notable that one row of cooling holes is located in DZ and their diameter is 0.6mm. The cooling holes are shown in "Fig. 5". In other words, it is a guarantee to ensure proper cooling in DZ.
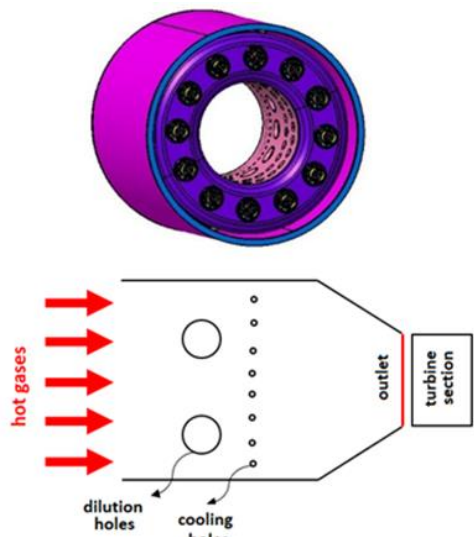

Fig. 5   The annular combustion chamber and the cooling holes in DZ.

It is necessary to study the reactive flow of combustion chamber. Quality of RZ formation and its details are investigated at RANS study. Numerical simulation has been done in ANSYS FLUENT. The RNG turbulent model and the finite rate/eddy dissipation combustion model have been used for simulation. The main assumptions of present work are listed as follows: 1) The fluid flow is incompressible, transient, three-dimensional, and turbulent. 2) Properties of the fluid flow are assumed to be constant. 3) The gravitational acceleration effects are neglected.

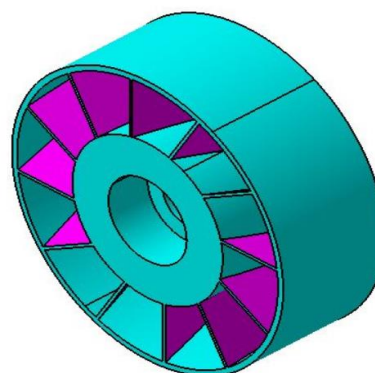Figure 6 shows the SW geometry of annular combustion chamber.

Fig. 6   The swirler geometry.

5   GOVERNING EQUATIONS

The 3D flow is assumed to be incompressible and turbulent. The continuity and the momentum Equations are presented with (17) to (18) respectively [21]:

$$\frac{\partial}{\partial t} + \frac{\partial}{\partial x_i}(\rho u_i) = 0 \tag{17}$$

$$\frac{\partial}{\partial t}(\rho u_i) + \frac{\partial}{\partial x_j}(\rho u_i u_j) =$$
$$-\frac{\partial P}{\partial x_i} + \frac{\partial}{\partial x_j}\left[\left(\frac{\partial u_i}{\partial x_j} + \frac{\partial u_j}{\partial x_i} - \frac{2}{3}\delta_{ij}\frac{\partial u_i}{\partial x_j}\right)\right] + \frac{\partial}{\partial x_j}\left(-\rho\overline{\acute{u_i}\acute{u_j}}\right) \tag{18}$$

The energy and the species transport Equations are modelled as follows Equation (18) and Equation (19) [22]:

$$\frac{\partial}{\partial t}(\rho E) + \frac{\partial}{\partial x_i}\left(u_i(\rho E + P)\right) =$$
$$\frac{\partial}{\partial x_j}\left[k_{eff}\left(\frac{\partial T}{\partial x_j}\right) + u_i\mu_{eff}\left[\left(\frac{\partial u_i}{\partial x_j} + \frac{\partial u_j}{\partial x_i}\right) - \frac{2}{3}\delta_{ij}\frac{\partial u_i}{\partial x_j}\right]\right] + S_r \tag{18}$$

$$\frac{\partial}{\partial t}(\rho u_i) + \frac{\partial}{\partial x_j}(\rho u_i u_j) =$$

$$-\frac{\partial P}{\partial x_i} + \frac{\partial}{\partial x_j}\left[\left(\frac{\partial u_i}{\partial x_j} + \frac{\partial u_j}{\partial x_i} - \frac{2}{3}\delta_{ij}\frac{\partial u_i}{\partial x_j}\right)\right] + \frac{\partial}{\partial x_j}\left(-\rho\overline{\hat{u}_i\hat{u}_j}\right) \quad (19)$$

Fuel $C_{12}H_{23}$ has been placed in the fuel database of the CFD software (FLUENT) which is named kerosene. Its reaction mechanism in the reaction mechanism database of this software is one step reaction mechanism and it is expressed in Equation (5) [23-24]. The activation energy is $1.257 *10^5$ J/mole.

6   NUMERICAL SIMULATION

A 30-degree cross-section is investigated, because of the symmetry of the combustion chamber. Generation of the unstructured hexahedral grid is done based on ICEM software. The SN approximately is equal to one. So, the grid must be generated as fine as possible. The grid structure of the combustion chamber is shown in "Fig. 7". In this research, accurate resolution of the boundary layer greatly affects the accuracy of the results, because the geometry of the swirler is complex and there are many vorticities with various dimensions in the combustion chamber. Figure 8 shows the boundary layer on the swirler vanes.
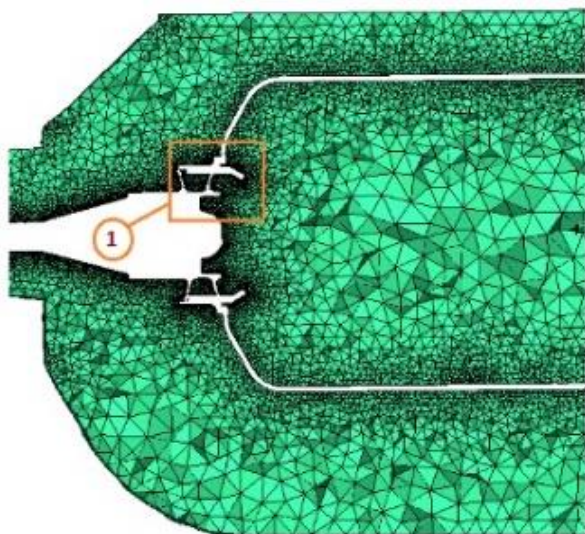

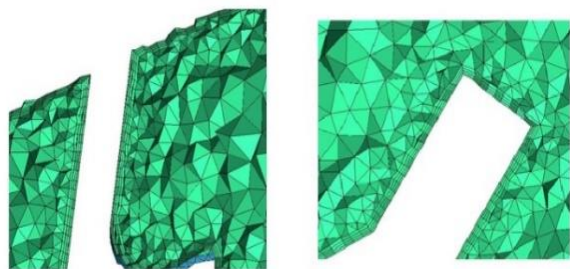**Fig. 7**   Grid in the basic design.

Fig. 8   Grid details in swirl vane.

The boundary conditions include mass flow rate at the inlet and static pressure at the outlet of combustion chamber. In addition, periodic boundary condition is employed at the symmetry planes. The atomizer is hollow cone type which is produced with average droplet diameter of 20 micrometres. Fluent software is employed to simulate this problem based on the finite volume method in the cell center, the flow is considered to be unsteady and incompressible [24]. The PISO method is used for Pressure and velocity coupling. The convergence criterion relative error for the Equation of mass conservation and for other Equations are 10^{-3} and 10^{-5}, respectively.

7   GRID STUDY

Three grids with the grid size of 1.52 million, 1.97 million and 2.66 million cells are used to achieve the grid independent results. The average temperature of 7 different cross-sections of the combustion chamber are compared in "Fig. 9".
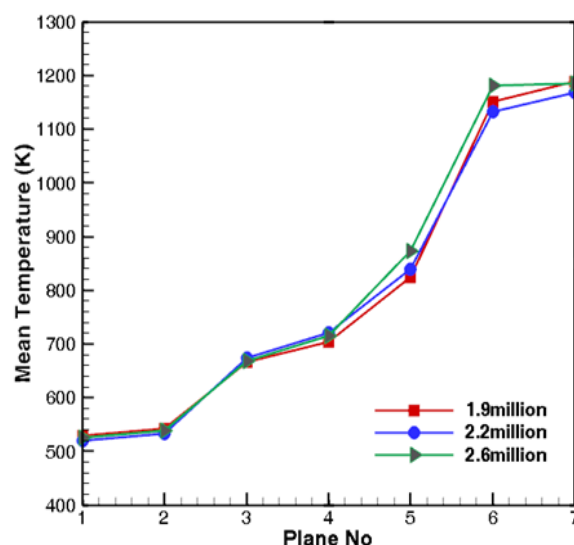

Fig. 9   Average temperature in different transverse planes versus the number of cells.

Based on "Fig.9", the temperature is between 5 K and 27 K in the identical design. Eventually the grid with 2.2 million cells was used to simulate the problem. Besides grid independency, the time step study must be done in the numerical solution. The basic design simulation was done at three-time steps of 1×10^{-5} sec, 1×10^{-6} sec and 1×10^{-7} sec. The results showed that the difference of average total temperature in all three-time steps is about 5 K, but the run time with a small time-step, has significantly increased. So, for the simulation of the three proposed designs, the time step of 1×10^{-5} sec was used. The boundary conditions are mass flow at the inlet

and static pressure at the outlet. Periodic condition is used at the symmetry faces.

8   EXPERIMENTAL SET UP

Figureee 10 shows experimental setup of the combustion chamber in present study. The blue trace of "Fig.10" is only used in cold flow test for measuring total pressure.
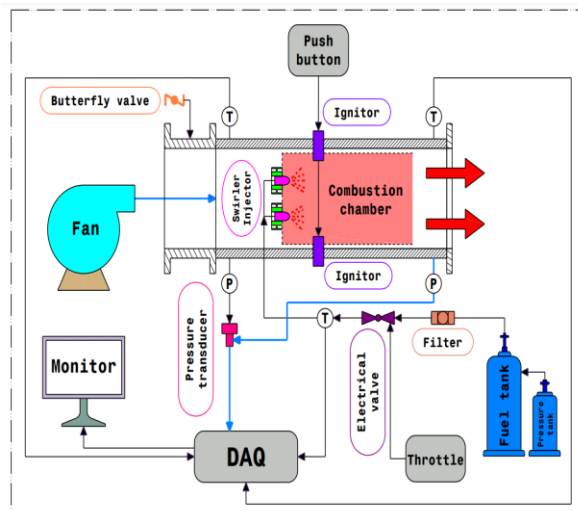

Fig. 10   Experimental setup of combustion chamber test rig in the present study.

This set up includes air system, fuel system and measuring equipment required. Note that the test rig is equipped with a butterfly valve that provides the conditions for atmospheric and pressurized experiment. A twin fan is used to supply air, which has a nominal speed of 3000 rpm. Fuel mass flow rate is also measured with an electric motor and solenoid valve. The output signal is transmitted to Data Acquisition (DA) and then the fuel mass flow rate is read. Two elements are used to start the combustion. These elements use electricity with a voltage of 30 V and 4.5 A current.

Figure 11 shows the combustion chamber test rig and the section model in the present study. The measuring equipment are installed in the inlet and outlet of the section model.

The pitot tube is used to measure total pressure and static pressure. Total temperature is measured at the inlet and outlet of the combustion chamber with thermocouples which are K type and B type, respectively.

The data acquisition system (DAQ) includes an electronic board for secure signal transmission to multipurpose cards. They have 16 analog input channels that can convert analog data to digital data. It should be noted that other parameters required for engine testing are considered in the DAQ.
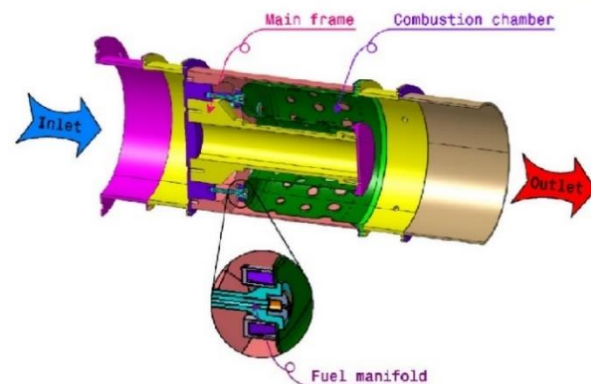

Fig. 11   The combustion chamber test rig and section model in present study.

"Table 4" shows the atmospheric test condition.

Table 4 Atmospheric test conditions

Zone	Range
P0(kPa)	101.7
T0(K)	288-310
Air mass flow rate (Kg/s)	0-1.2
Fuel mass flow rate (Kg/s)	0-0.03

The experimental procedure is divided into cold flow test and hot flow test. The pressure loss in cold flow test and average outlet total temperature of the combustion chamber are measured in hot flow test. The inlet conditions of the combustion chamber for the ATR should be set to those MFP values which have the same value as the engine case under elevated pressure conditions. MFP for both cases are:

$$\text{MFP}_{\text{engine}} = \frac{\dot{m}_{\text{air,in}} T_{\text{tot,in}}^{0.5}}{P_{\text{tot,in}}} \tag{21}$$

$$\text{MFP}_{\text{Rig}} = \frac{\dot{m}_{\text{air,atm}} T_{\text{tot,atm}}^{0.5}}{P_{\text{tot,atm}}} \tag{22}$$

The fuel mass flow rates for ATR is calculated based on Equation (23):

$$\dot{m}_{\text{f,atm}} = \dot{m}_{\text{air,atm}} \text{FAR} \tag{23}$$

Experimental investigation is performed for different operating conditions of the annular combustion chamber based on "Table 5".

Table 5 Different operating conditions for comparison experimental and numerical results

Case Number (C.N)	MP	FAR
1	0.1206	0.0125
2	0.1397	0.0178
3	0.1642	0.0092
4	0.1736	0.0145
5	0.1754	0.0085
6	0.2004	0.0123

The pressure loss is calculated by the use of Equation (24). $P_{0,in}$ and $P_{0,out}$ are inlet and outlet total pressure in cold flow, respectively.

$$\Delta P_{cf}\% = \left| \frac{P_{0,out} - P_{0,in}}{P_{0,in}} \times 100 \right| \qquad (24)$$

9   VALIDATION AND VERIFICATION

Numerical simulation for 6 different cases of table 6 was done based on method of section 4. The error percentage of cold pressure loss and TIT are based on Equation (25) and (26), respectively.

$$\text{Error}\% = \left| \frac{\Delta P_{0,exp}\% - \Delta P_{0,CFD}\%}{\Delta P_{0,exp}\%} \times 100 \right| \qquad (25)$$

$$\text{Error}\% = \left| \frac{TIT_{exp} - TIT_{CFD}}{TIT_{exp}} \times 100 \right| \qquad (26)$$

The results of cold pressure loss and TIT were shown in "Table 6" and "Table 7", respectively.

Table 6 Comparison of the numerical analysis with the experimental results of pressure drop of non-reacting flow in percentage

(C.N)	$\Delta P0_{cf}\%$-Exp	$\Delta P0_{cf}\%$-CFD	Error%
1	0.2262	0.2321	2.6235
2	0.2298	0.2778	3.8726
3	0.8517	0.8276	2.8314
4	0.1942	1.0360	4.7624
5	1.7373	1.8157	4.5127
6	1.9183	1.8825	2.0602

Table 7 Comparison of experimental measurements and numerical estimation of TIT values at different operating conditions.

C.N	TIT-Exp	TIT-CFD	ΔTIT(K)	Error%
1	760	769.77	9.77	1.28
2	955	949.53	5.47	0.57
3	675	666.85	8.15	1.20
4	855	862.62	7.62	0.89
5	666	645.60	20.4	3.06
6	745	749.52	4.52	0.60

10   RESULT

Figure 12 shows the pattern formation of IRZ and ORZ. The high quality of IRZ and ORZ shows that swirler creates powerful swirling flow.
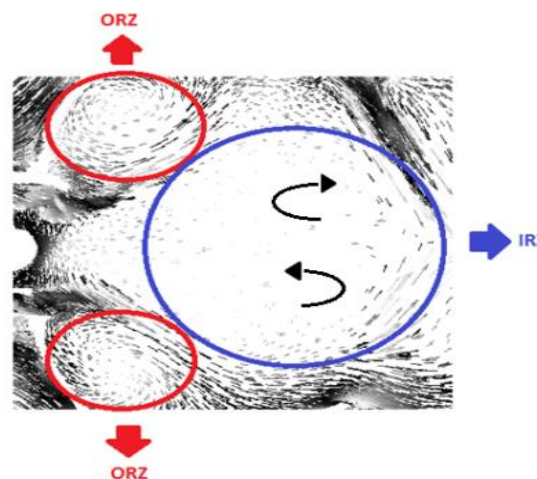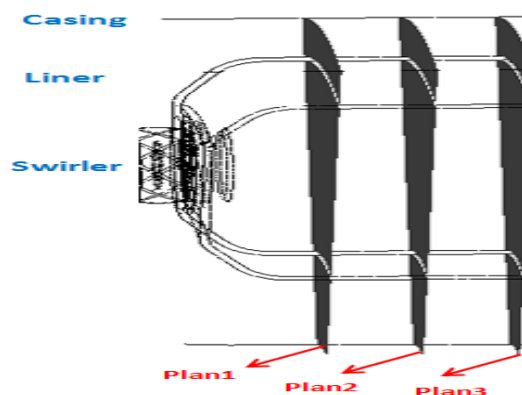

Fig. 12   The pattern formation of IRZ and ORZ.

Figure 13 illustrates the position of the three plates which are located at the first, center and end of the RZ. The total temperature contour at three plans are shown in "Fig. 13".

Fig. 13   The position of the three plates at the first, center and end of the RZ.

The total temperature contour at (a) the first plane, (b) the central plane, (c) the end plane based on "Fig. 13" are shown in "Fig. 14". The average total temperature of the core are 1004K, 1011K and 1023K, respectively. Average total temperature at the RZ is approximately constant. The strong swirling flow is created in the annular combustion chamber, because of the difference of 19K from the first to the end of the RZ. The maximum total temperature at the are 2344K, 2313K and 2352K, respectively. The quality of the temperature distribution in the RZ is an important point. It indirectly refers to the fuel-air mixing quality. Comparison of the temperature contours in "Fig. 14" shows that the temperature uniformity is gradually improved in RZ.
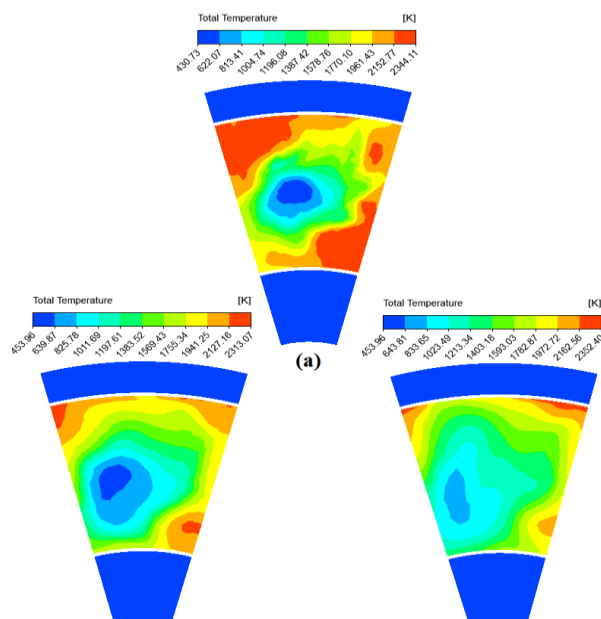

Fig. 14 The total temperature contour at: (a): the first plane, (b): the central plane, and (c): the end plane based on "Fig. 13".

The comparison of air partitioning in design and CFD results is shown in "Table 8".

Table 8 The comparison of air partitioning in 1DD and CFD results

Zone	Air mass flow rate% in design	Air mass flow rate% in CFD	Error%
CZ	20	19.82	0.90
SZ	12	11.74	2.16
DZ	68	68.44	0.64

Figure 15 shows the total outlet temperature of combustion chamber. The average and maximum output temperature are 1191.7K and 1416K, respectively. The formation of the hot core at the center of the combustion chamber section is remarkable. Although the temperature in the vicinity of the inner liner has reached

1416K, the combustion chamber is made of Hastelloy alloy [25].
It is defined based on Equation (27) [1]:

$$PF = \frac{T_{tot,max,out} - T_{tot,ave,out}}{T_{tot,ave,out} - T_{tot,in}} \tag{27}$$

In Equation (44), $T_{tot,max,out}$, $T_{tot,ave,out}$, and $T_{tot,in}$ represent the maximum total outlet temperature, the average total outlet temperature, and the inlet total temperature of the combustion chamber, respectively. PF quantity is 0.31.
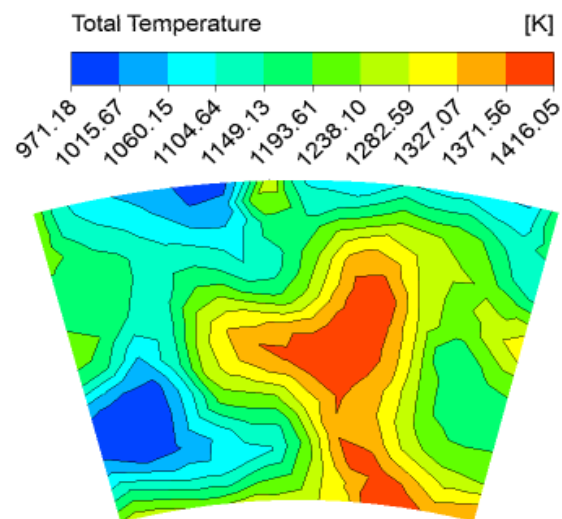

Fig. 15 The Contour of outlet total temperature.

The pressure loss is calculated based on Equation (28) [1]. $P_{0,in}$ and $P_{0,out}$ are inlet and outlet total pressure.

$$\Delta P\% = \frac{P_{0,out} - P_{0,in}}{P_{0,in}} \times 100 \tag{28}$$

The pressure loss is 6.70% based on CFD result and Equation (28). The error percent between the amount of pressure loss in design and CFD result is 1.07%.

11 CONCLUSIONS

In this study, an annular combustion chamber of a turbojet engine with 1650N thrust and kerosene as fuel to achieve the SN was investigated. The key following results were obtained and conclusions should state concisely the most important propositions of the paper as well as the author's views of the practical implications of the results.

1- SN is equal to 0.9955 in design process. It indicates the design methodology of combustion chamber is appropriate to achieve the maximum SN. The ORZ and IRZ formation in CFD results verified that the SW geometry design is compatible with others section of combustion chamber.

2- The maximum total temperature at the first, center and the end of RZ are 2344K, 2313K and 2352K, respectively. The temperature distribution of RZ shows that the temperature uniformity is gradually improved in RZ.

3- CFD study indicates that the temperature distribution at the outlet of combustion chamber is relatively uniform, and the average total outlet temperature is 1191.7K. It is close to the desired value of total outlet temperature in design.

4- The PF is 0.31 in CFD result and it is estimated 0.25 in design. The error between two values is 24%. It is a positive point, because the design methodology is able to produce more uniform outlet temperature profile.

5- The pressure loss is 6.57% based on CFD result. The error percent between the amount of pressure loss in design and CFD result is 1.07%. The error percent of air partitioning in design and CFD results are 0.90%, 2.16% and 064% in CZ, SZ, and DZ, respectively. It shows that the design methodology is efficient.

6- The RNG turbulence model is a suitable model for trapping small vortices. It also indicates the proper coupling of the RNG model and the species transport combination model.

7- Experimental study is recommended to ensure that the performance quality of the designed combustion chamber is high enough to gain the desired thrust. For future work, the atmospheric test will be studied until high performance is gained.

REFERENCES

[1] Lefebvre, A. H., Ballal, D. R., Gas Turbine Combustion: Alternative Fuels and Emissions, 3rd ed, CRC press, 2010, Chap. 4.

[2] Mattingly, J. D., Heiser, W. H., and Pratt, D. T., Aircraft Engine Design, American Institute of Aeronautics and Astronautics, 3rd ed, American Institute of Aeronautics and Astronautics, Inc., Reston 2002, Chap. 9.

[3] Mellor, Design of Modern Turbine Combustors, Academic Press, 1990, Chaps. 1, 4.

[4] Mohammed, R. S. E., Design and Analysis of Annular Combustion Chamber for a Micro Turbojet Engine, International Journal of Aerospace and Mechanical Engineering, Vol. 13, No. 4, 2019, pp. 282-287.

[5] Mark, C. P., Selwyn, A., Design and Analysis of Annular Combustion Chamber of a Low by Pass Turbofan Engine in a Jet Trainer Aircraft, Propulsion and Power Research, Vol. 5, No. 2, 2016, pp:97-107.

[6] Zeng, Q., Yuan, Y., Flow Dynamics of Dual-Stage Counter-Swirl Combustor in Different Confinement Spaces, International Communications in Heat and Mass Transfer, Vol. 116, 2020, pp. 104633.

[7] Jiang, Y., Yue, G., Dong, P., Gao, J., and Zheng, Q., Investigation on Film Cooling with Swirling Coolant Flow by Optimizing the Inflow Chamber, International Communications in Heat and Mass Transfer, Vol. 88, 2017, pp. 99-107.

[8] Saboohi, Z., Ommi, F., and Akbari, M. J., Multi-Objective, Optimization Approach Toward Conceptual Design of Gas Turbine Combustor, Applied Thermal Engineering, Vol. 148, 2019, pp. 1210.

[9] Amani, E., Rahdan, P., and Pourvosoughi, S., Multi-Objective Optimizations of Air partitioning in a Gas Turbine Combustor, Applied Thermal Engineering, Vol. 148, 2019, pp. 1292-1302.

[10] Treedet, W., Suntivarakorn, R., Effect of Various Inlet Geometries on Swirling Flow in Can Combustor, Journal of Mechanical Engineering and Sciences, Vol. 12, 2018, pp. 3712-3723.

[11] Eldrainy, Y. A., Saqr, K. M., Aly, H. S., Lazim, T. M., and Jaafar, M. N. M., Large Eddy Simulation and Preliminary Modeling of the Flow Downstream a Variable Geometry Swirler for Gas Turbine Combustors, International Communications in Heat and Mass Transfer, Vol. 38, No. 8, 2011, pp. 1104-1109.

[12] Eldrainy, Y. A., Saqr, K. M., Aly, H. S., Lazim, T. M., Jaafar, M. N. M., CFD Insight of the Flow Dynamics in a Novel Swirler for Gas Turbine Combustors, International Communications in Heat and Mass Transfer, Vol. 36, No. 9, 2009, pp. 936-941.

[13] Chen, R. H., Driscoll, J. F., The Role of the Recirculation Vortex in Improvement Fuel- Air Mixing within Swirling Flames, Processing in Symposium (International) on Combustion, Vol. 22, No. 1, 1989, pp. 531-540.

[14] Liu, Y., Zhang, L., Chen, Z., and Zhou, L., Numerical Investigation on Mixture Particle Dispersion Characteristics in Swirling Particle-laden Combustion Chamber, International Communications in Heat and Mass Transfer, Vol. 117, 2020, pp.104720.

[15] Çakmak, G., Yıldız, C., The Influence of the Injectors with Swirling Flow Generating on the Heat Transfer in the Concentric Heat Exchanger, International Communications in Heat and Mass transfer, Vol. 34, No. 6, 2007, pp. 728-739.

[16] Torkzadeh, M., Bolourchifard, F., Amani, E., An Investigation of Air-Swirl Design Criteria for Gas Turbine Combustors through a Multi-Objective CFD Optimization, Fuel, Vol. 186, 2016, pp. 734-749.

[17] Pourfarzaneh, H., Modelling of Turbojet Propulsion Performance and Experimental Validation, Ph.D. dissertation, Dept. Mech. Eng., Sharif Univ., Tehran, Iran, 2010.

[18] Conrado, A. C., Locava, P. T., Filho, P., and Sanchez, M. S., Basic Design Principles for Gas Turbine Combustor, Processing of the 10th Brazilian Congress of Thermal Science and Engineering, Riodejaneiro, 2004.

[19] Khandelwal, B., Lili, D., and Sethi, V., Design and Study on Performance of Axial Swirler for Annular Combustor by Changing Different Design Parameters, Journal of the Energy Institute, Vol. 87, No. 4, 2014, pp. 372-382.

[20] Saboohi. Z., Ommi. F., and Fakhrtabatabaei, A., Development of an Augmented Conceptual Design Tool for Air Craft Gas Turbine Combustors, International Journal of Multiphysics, Vol. 10, 2016, pp. 53-73.

[21] Ajmi, M., Hnaien, N., Marzouk, S., Kolsi, L., Ghachem, K., Aissia, H. B., and Almeshaal, M. A., Numerical Investigation of Heat Transfer Enhancement of an Inclined Heated Offset Jet, International Communications in Heat and Mass Transfer, Vol. 116, 2020, pp. 104682.

[22] Luan, Y. T., Chuou, Y. P., and Wang, T., Numerical Analysis of Gasification Performance via Finite-Rate Model in a Cross-Type Two-Stage Gasifier, International Communication in Heat and Mass Transfer, Vol. 52, 2013, pp. 558-566.

[23] Zeng, W., Liang, S., Li, H. X., and Ma, H. A, Chemical Kinetic Simulation of Kerosene Combustion in an Individual Flame Tube, Journal of Advanced Research, Vol. 5, 2014, pp. 357-366.

[24] ANSYS Fluent Tutorials, Release 16, Ansys inc, 2015.

[25] Montero Sistiagoa, M. L., Pourbabak, S., Humbeeck, J. V., Schryvers, D., and Vanmeensel, K., Micro Structure and Mechanical Properties of Hastelloy X Produced by HB-SLM (High Power Selective Laser Melting), Materials & Design, Vol. 165, 2019, pp. 107598.